Soft Matter

RSC Publishing

PAPER

View Article Online
View Journal | View Issue

Cite this: *Soft Matter*, 2013, **9**, 6515

Crack propagation at the interface between soft adhesives and model surfaces studied with a sticky wedge test

Satyam Bhuyan,[a] François Tanguy,[a] David Martina,[a] Anke Lindner,[b] Matteo Ciccotti*[a] and Costantino Creton*[a]

The motion of the triple line during the debonding of a soft viscoelastic adhesive from a rigid polymer surface has been investigated quantitatively. In order to make the debonding geometry simpler than the probe tack test, a new technique, called the sticky wedge test, has been developed where the probe is constituted by a horizontal cylinder instead of a flat punch. The crack propagates in the elongated contact area between the cylinder and the flat surface, thereby, allowing us to measure optically *in situ* the crack-tip velocity and the receding contact angle of the debonding adhesive. Two model pressure sensitive adhesives (PSA) based on poly(*n*-butyl acrylate-*co*-acrylic acid) with different molecular weights and branching levels and four polymer substrates (rubbery or glassy at room temperature) were used. Due to the soft and incompressible nature of the adhesive, the strain energy release rate for this test geometry has been estimated by the equations for the pure shear test geometry. The results show three main new insights: first, despite significant approximations, this novel approach holds promise to characterize more *quantitatively* the interfacial crack propagation between soft viscoelastic solids and hard surfaces and the relationship between the applied energy release rate $\mathcal{G}$ and the crack-tip velocity v has been reliably established for eight combinations of the model viscoelastic adhesives and surfaces. Second, at equivalent values of the thermodynamic work of adhesion, the adhesion energy of both the adhesives against the rubbery surface was much lower than that against the glassy polymers. Third, surprisingly, the measured receding contact angle of debonding was close to 90° for all adhesive/surface combinations used.

Received 20th December 2012
Accepted 20th May 2013

DOI: 10.1039/c3sm27919g

www.rsc.org/softmatter

1 Introduction

Adhesion of soft materials is of great importance in several technologies.[1] In applications where high bond strength is not required, PSA have gained continuous market-share due to their safe handling, for both the consumer and the manufacturer.[2] Yet in particular, in some high-tech applications, controlling precisely the adhesive property is crucially important. Despite some important recent advances in the understanding on how PSA detach from surfaces,[3–6] one of the outstanding problems is the treatment of the boundary condition at the interface between the soft viscoelastic material and a hard surface. Numerous theories have been developed in the last forty years to explain the adhesion and the interfacial fracture of elastic fully crosslinked soft rubbers[7–16] and have typically treated the interfacial boundary condition either as a reversible break up of van der Waals bonds (represented by the thermodynamic work of adhesion), or as an irreversible failure of covalent bonds by the Lake-Thomas mechanism.[14,15] In both cases, however, the failure occurs by a simple mechanism of crack propagation. Softer and highly viscoelastic PSA, on the other hand, generally deform significantly during debonding and fail by more complex mechanisms involving both the interface and non-linear bulk deformations.[10,11,17,18]

More specifically, the adhesive can either detach by propagation of cracks at the interface or can form long bridging fibrils in the bulk during the detachment. The final detachment itself can either be interfacial when fibrils are eventually peeled off the surface, or cohesive, leaving residues on the surface.[12] While most of the past studies have focused on fibrillating PSA and have used peel test or probe tack methods,[12,18–27] there are only a few experimental studies on crack propagation between *viscoelastic* materials and hard surfaces.[28–30]

To perform a systematic study on the debonding mechanisms, the requirements are a material system with controllable viscoelastic properties, a well characterized hard surface, and a

[a]*Laboratoire de Sciences et Ingénierie de la Matière Molle, UMR 7615, ESPCIParisTech-UPMC-CNRS, 10 Rue Vauquelin, 75231 Paris Cédex 05, France. E-mail: matteo.ciccotti@espci.fr; costantino.creton@espci.fr*

[b]*Laboratoire de Physique et Mécanique des Milieux Hétérogènes, UMR 7636, ESPCI ParisTech- Univ Paris Diderot – UPMC - CNRS, 10 Rue Vauquelin, 75231 Paris Cédex 05, France*

reproducible debonding test in a simple geometry. A previous study used a 3D visualization set-up, allowing for the first time a quantitative measurement of the shape of the crack[11] and the receding contact angle[10] between a soft material and a solid surface during debonding from a circular flat-ended probe. Because PSA are viscoelastic the dissipated energy per unit area of crack will depend on the crack velocity. However, the circular geometry and the complex crack propagation pattern (including cavitation or fingering) in the probe tack method made it impossible to estimate accurately the relationship between the elastic energy released by the deformed adhesive and the resulting local crack velocity, which is spatially heterogeneous.

To address this limitation, a different technique has been developed in this study in which both the deformation imposed on PSA films and the crack velocity can be measured by examining the geometry and the free boundaries of the deforming film. To make both the visualization and the modelling easier, this technique uses a pseudo-2D contact and a debonding geometry where the edge of a crack propagates like a strip loaded in pure shear, *i.e.* at a constant value of the energy release rate $\mathcal{G}$. The position of the crack-tip can be tracked and the shape of the contact line can be extracted from the images obtained using high magnification cameras. Using MATLAB routines, it is possible to measure the velocity v and the contact angle θ of the moving crack. Since adhesive properties of soft adhesives are clearly related to their viscoelastic properties,[20,31,32] small strain rheological characterization was also performed using a shear rheometer.

2 Materials and methods

2.1 Materials

In order to study the interfacial debonding of PSA quantitatively, an appropriate choice of adhesives and surfaces is critical. If the adhesive is too liquid-like then cracks will be pinned and the debonding will occur by fibrillation, whereas if the adhesive is too elastic its adhesion energy will be low and not representative of PSA. Likewise, the surface and the experimental geometry should be such that the adhesive is capable of undergoing interfacial debonding mainly through crack propagation without any fibrillation or extensive multiple cavitations.

The two adhesive samples used in this study are random copolymers with a low glass transition temperature, whose constituents are 98% butyl acrylate and 2% acrylic acid. They were obtained by drying of latexes provided by The Dow Chemical Company. The latex was left to dry on a PET film for 48 h in air in an oven overnight. The thickness of the adhesive film was around 100 ± 15 μm in the fully dry state. The two adhesives have been labelled as Bg1110 and B1080 throughout the text with the number representing their average molecular weight in thousands of grams per mole. Both materials were synthesized by emulsion polymerization and have a weight average molecular weight of the soluble fraction of 1080 kg mol^{-1} and 1110 kg mol^{-1} respectively and a polydispersity $I_p = 1.82$. The key difference between the two polymer films is that Bg1110 contains 30% (w/w) of insoluble fraction in tetrahydrofuran (THF), and hence the 'g' for gel, while B1080 is fully soluble. As a result, Bg1110 is more elastic and crosslinked than B1080.

Table 1 Glass transition temperature T_g and the wetting contact angle θ with water for the adhesives and the surfaces used in this study

Samples	T_g (°C)	Θ (degrees)[d]
Adhesives		
Bg1110	−40[a]	93
B1080	−40[a]	92
Surfaces		
PIB	−64[b]	93
COC	80[b]	93
PMMA	105[c]	80
PS	95[c]	94

[a] Measured using differential scanning calorimetry. [b] Specified by manufacturer. [c] From ref. 38. [d] Obtained from equilibrium wetting tests performed in the present study with an error of ±2°, which does not allow us to differentiate advancing and receding contact angles.

Four different flat surfaces were used with different surface compositions. They were: (1) polyisobutylene (PIB) (Sigma-Aldrich), (2) a glassy cyclic olefin random copolymer consisting of polyethylene and 64% (w/w) norbornene (labelled COC) (TOPAS®Advance Polymers, Frankfurt, Germany), (3) polystyrene (PS) (Sigma-Aldrich) and (4) poly(methylmethacrylate) (PMMA) (Sigma-Aldrich). The glass transition temperature T_g of the materials constituting the adhesives and the surfaces is reported in Table 1. All surfaces were prepared by spin coating 1% (w/w) solution in toluene on a 2 mm microscope glass slide. This resulted in a substrate coated with a transparent homogenous layer with an approximate thickness of 1 μm.

2.2 Rheology of model PSA

The linear viscoelastic properties of the model adhesives were characterized with a strain-controlled rheometer (ARES, TA Instruments) using circular parallel-plate tools with plate diameter 8 mm, at frequencies between 10^{-2} and 10^{2} rad s^{-1}, and at temperatures between −30 °C and 90 °C. The dynamic viscoelastic moduli were characterized in the linear regime by frequency sweeps at 5% strain and the variations of the complex moduli with frequency at a reference temperature of 30 °C were obtained by constructing time–temperature superposition master curves using WLF shift parameters.[33,34]

The storage modulus G', the loss modulus G'' and their ratio $\tan(\delta) = \frac{G''}{G'}$ were obtained as a function of the angular frequency ω. Values of G' and $\tan(\delta)$ as a function of ω for both the materials are shown in Fig. 1(a) and (b) respectively. A good PSA has a dynamic shear modulus G' lower than 0.1 MPa at 1 Hz and a value of $\tan(\delta)$ between 0.2 and 0.5.[2] This empirical criterion can be understood simply as a criterion for establishing a good molecular contact even on rough surfaces[35] and for dissipating sufficient energy upon debonding and it is met by our model PSA. At low frequency, the values of G' for Bg1110 are higher than B1080 which mainly indicates the more

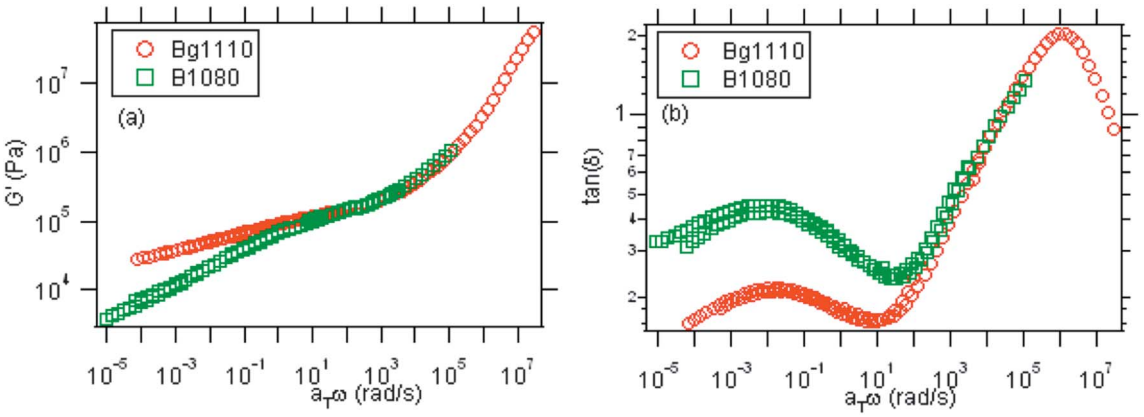

Fig. 1 Linear viscoelastic characterization of the adhesives Bg1110 and B1080 (master curves at a reference temperature of 30 °C) showing the values of (a) the dynamic storage modulus G' and (b) the loss factor tan(δ) against the frequency of shear.

crosslinked structure of the adhesive containing the gel fraction. The tan(δ) values of B1080 at low frequency are higher than those of Bg1110 indicating that it dissipates more energy viscoelastically upon deformation.

2.3 Crack propagation with the sticky wedge test

In order to investigate the crack propagation at the interface of the adhesive and the adherent, a strip of adhesive is brought into contact with the glass slide and is then debonded from the latter. As described in Fig. 2 and 3, the set-up consists of a steel cantilever beam with one end chiselled into the shape of a wedge while the other end is fixed to a moving stage. A uniform layer of dried adhesive of thickness 100 ± 15 μm deposited on a plasma-treated PET film of thickness 50 μm goes around a pin of 800 μm in diameter and is clamped to both sides of the beam. The stage moves biaxially allowing the adhesive to come in contact with the desired surface which as mentioned in the previous section is the polymer coated transparent substrate. The wedge-end of the beam along with the adhesive layer and the substrate is sketched in Fig. 2. The length of the adhesive strip that is exposed to the substrate is about 5 cm. The substrate is kept fixed while the motion of the wedge, and hence the relative position between the adhesive and the surface, is manually controlled by a micrometer screw of resolution 1 μm. Multiple tests were carried out at different relative locations of the sample and the substrate, constituting a total of up to 12 tests for each sample/substrate combination. Each test is performed in the following way: the adhesive film is first slowly brought close to the substrate until it snaps into contact. This snap into contact is used to define the reference point of the displacement δ of the micrometer screw for that particular experiment and hence for the calculation of the energy release rate. As soon as the film sticks, a small compression corresponding to a displacement of ~3 μm of the screw is manually given. This ensures uniform contact on the substrate which reaches equilibrium immediately with a finite contact length (close to 5 cm) and width (of the order of the film thickness, *i.e.*; 100–200 μm). The film is then retracted from the substrate to a set value of the displacement δ (different for every experiment and defined by the user, ranging from $0 < \delta < 60$ μm) by a manual motion of the screw and it is kept at that position for the rest of the test while the video recording is started. The procedure is designed to simulate a sudden loading of the adhesive strip inducing a crack propagation with a fixed value of the energy release rate.

As the adhesive film is retracted from the substrate to the set value of the displacement δ, the width of the contact shrinks to a smaller value (ranging between 10 and 20 μm), then the applied

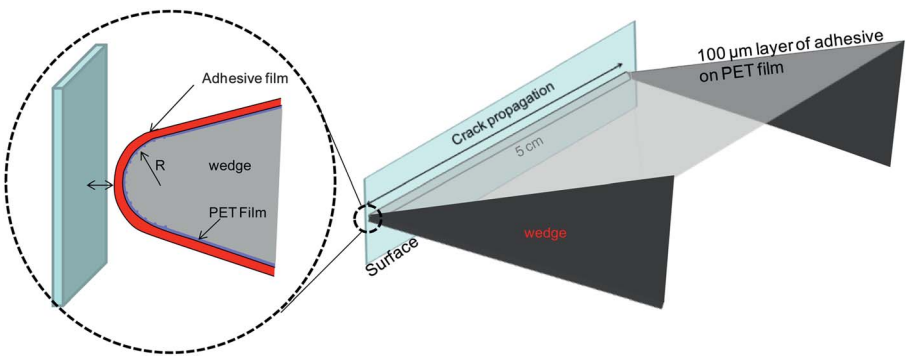

Fig. 2 Sketch showing a layer of adhesive film of thickness ~100 μm deposited on a PET film being rolled over a wedge and brought in contact with the surface.

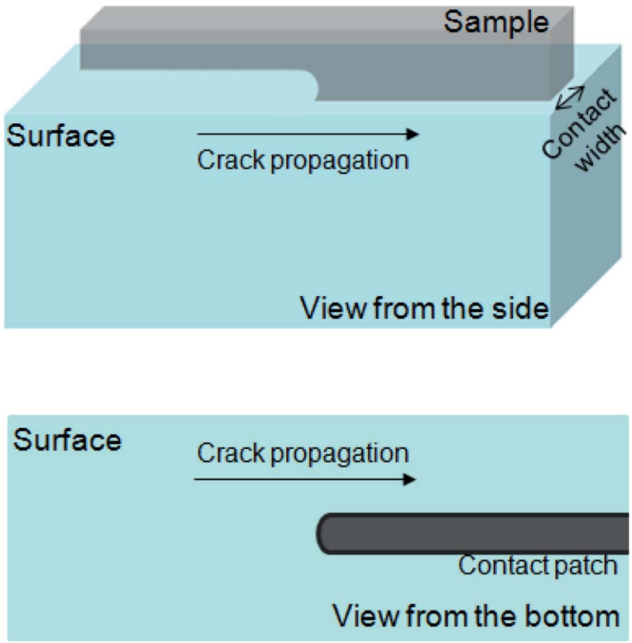

Fig. 3 Two sketches of a single propagating crack directly observed from the side and the bottom cameras in Fig. 2. As the adhesive is retracted from the surface to a fixed displacement, cracks nucleate at a certain point and propagate along the length of the contact patch. The side camera allows a quantitative analysis of the crack opening profile and the bottom camera is useful to observe the shape of the contact patch.

stress causes some cracks to nucleate at the interface and propagate along the length of the wedge which is the debonding line. The location of nucleation of the cracks is not *a priori* predictable for a new sample but when repeated contact and retraction experiments are made on the same sample (at different values of the applied displacement of the micrometer screw), the cracks nucleate in the same location. We do not focus on nucleation here, but rather on crack propagation, which occurs at a nearly constant velocity for a given applied displacement, and thus for a given constant value of the energy release rate due to the pure shear geometry (*cf.* later section).

During this process the debonding is visualised from the side and the bottom with two high magnification cameras as shown in the schematics of Fig. 3. The cameras are triggered simultaneously to capture images for further analysis. The side camera allows us to observe these cracks as they propagate along the debonding line. This is useful in order to characterize the crack geometry and quantify the crack-tip velocity and the contact angle. On the other hand, through the bottom camera one can see the contact region between the adhesive and the transparent substrate. This view provides important information for a qualitative analysis of the contact region when the adhesive is separated from the surface and will be used to justify the assumptions used for the modelling in Section 3.2.

3 Experimental results

3.1 Measurement of crack velocity

Fig. 4 shows a representative snapshot of the crack geometry between Bg1110 and PMMA as observed from the side camera. Here, one can see that one crack nucleates at a certain point indicated by the cross sign "×" and propagates in both directions. The two crack-tips are labelled as 1 and 2. The crack 2 which is moving rightward will eventually interact and coalesce with crack 3, which originates from a different nucleation point and is propagating in the opposite direction. The crack 1, which is moving leftwards, will also coalesce with another crack that is not visible in the frame. The distance that each crack traverses before coalescing with another crack is pre-determined by the spatial distribution of the crack nucleation points along the wedge. In Fig. 5, the positions of the crack-tips 2 and 3 from Fig. 4 have been determined by image analysis and the (positive) crack extension x after the nucleation point is plotted as a function of the propagation time t. One can see that the crack extension is roughly linear with time implying an approximately constant velocity, as expected. Some velocity changes are observed when two cracks approach each other, but this is clearly attributed to interaction before coalescence. For example, crack 3 which propagates over a longer distance maintains a steady propagation for some time and then jumps to coalescence. A similar behaviour is also seen in the case of crack 2 except that it propagates over a much shorter distance before coalescence. We can thus retain a single value of the average velocity for each crack, corresponding to the linear fits that are shown as dashed lines in Fig. 5. It can be seen in Fig. 5 that the average velocities for different cracks present some differences. These differences are reproduced when the test is repeated. They result from spatial heterogeneities in the test geometry or in the adhesive itself and are particularly marked for the example chosen in Fig. 5, corresponding to a substrate with strong adhesion (the glassy polymer PMMA). These differences are small when compared to the velocity variations as a function of δ, covering more than two decades. In order to obtain the best estimate of the variation of crack velocity with energy release rate, we thus decided to always choose the longest crack (crack 3 in the case of Fig. 5) as it provides the widest region with constant velocity. We then measure the changes of crack velocity as a function of the applied displacement δ.

Fig. 4 Representative image of the observation from the side camera showing three crack-tips of Bg1110 against PMMA as the adhesive is separated from the substrate after applying a fixed imposed displacement. The crack-tips have been labelled as 1, 2 and 3 with the directions indicated by the arrows. The white region at the interface is a reflection of the light shined on the adhesive. The positions of the crack 2 and crack 3 have been traced and plotted as a function of time in Fig. 5.

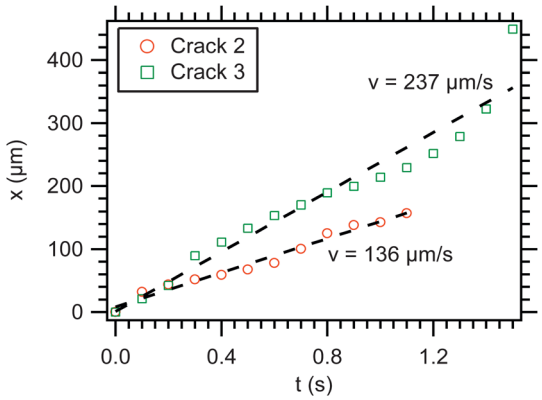

Fig. 5 Representative plots of the positions of the crack-tips 2 and 3 in Fig. 4 as a function of time. The linear fits are indicated by the dashed lines the slopes of which give the average velocities of the two crack-tips.

3.2 Estimation of the energy release rate

The given confined pseudo 2D geometry (Fig. 6) and the linear viscoelastic properties of the adhesive can be used to make a crude but useful estimate of the energy release rate. Since our testing conditions do not involve external work of the loading fixture, the energy release rate $\mathcal{G}$ is essentially a balance of the elastic energy changes following the crack propagation over a unit area. The viscoelastic response of the adhesive after the rapid initial loading is mainly a weak and slow relaxation. The energy release rate can thus be soundly approximated by using the calculations for an elastic soft solid, and taking an equivalent elastic modulus (the detailed procedure is explained below). The energy release rate $\mathcal{G}$ is calculated by assuming that the adhesive in the contact region is uniformly strained like a vertical strip. This geometry of a long thin strip is very classically used in fracture testing of rubber.[36] It has a distinct advantage that as the crack propagates along the strip the energy release rate does not change with crack length. This property can be easily understood by looking at the crack profiles in Fig. 3 and 4. Considering the propagation of an individual crack tip, we can identify three different regions: a uniformly strained strip ahead of the crack tip, an inhomogeneous region around the crack tip, and a substantially unloaded strip behind the crack tip. Since the energy in the inhomogeneous region remains essentially constant during steady-state propagation, the energy balance is given by the loss of the energy stored in the strip per unit area of crack advance. This can be approximated by multiplying an estimated value of the elastic energy density in the strip, by its height. The loading is thus substantially equivalent to the pure shear test geometry, and the energy release rate is given by:[36]

$$\mathcal{G} = 2G'\left(\frac{\delta}{h_0}\right)^2 (h_0 + \delta) \quad (1)$$

where h_o is the unstressed height of the adhesive film, δ is the displacement imposed on the adhesive from the reference first contact position and G' is the dynamic storage modulus in shear. The relationship $E' = 4G'$ was used to relate the shear modulus measured using the rheometer to the elastic modulus for a laterally constrained strip in pure shear assuming deformation at constant volume.

As viscoelastic relaxation is slow, we assume that the instantaneous value of G' of the two model adhesives needed in eqn (1) is well represented by the linear rheology measurements discussed in Section 2.3 and we estimate a single value of the dynamic storage modulus $G'(\omega^*)$ for each test. Here, we estimate the relevant frequency to be $\omega^* = \frac{2\pi}{t^*}$ with t^* being the duration of the test, which is mainly given as the time between the application of the displacement δ and the full detachment of the joint after crack propagation. This time t^* ranged from 0.1 to 60 s in this study. Eqn (1) is thus based on three important assumptions:

(I) The energy release rate is independent of crack length which implies a contact area that is much longer than its width.

(II) The linear elastic modulus of the material can be substituted by the time dependent dynamic storage modulus in shear G' measured at the appropriate frequency in shear rheology experiments.

(III) The proportionality constant between the shear modulus and the actual stiffness of the material above the contact is 4, which assumes that the material forms a vertical wall with the same cross-section as the contact area.

Assumption (I) is experimentally well verified due to the geometry of contact as discussed above. Assumption (II) is more questionable particularly in view of the approximation made above for the frequency ω^*. However, when comparing the duration of the tests (between 0.1 and 60 s) with the time-dependent rheological properties of our viscoelastic adhesives (Fig. 1), we can assume that ahead of the crack, the stored elastic energy is only reduced by a slow relaxation over a time corresponding to the time elapsed after the initial loading, while this elastic energy rapidly reduces to zero behind the crack, thus confirming the proposed energy balance. Finally, assumption (III) is the most questionable since the volume above the contact patch from which the elastic energy is

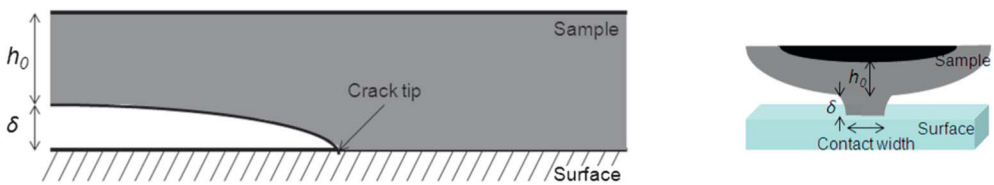

Fig. 6 (left) Sketch showing a crack propagating rightwards as observed from the side. (right) Sketch showing the cross-section of the contact region. h_0 is the original thickness of the soft adhesive film, δ is the initially imposed displacement between the sample and the surface resulting in a large strain of the soft adhesive along this contact region.

released to propagate the crack cannot be as simple as a vertical wall. However, once the contact region is strongly strained as in Fig. 4, its shape becomes indeed very close to a vertical wall. This particular approximation will tend to underestimate all values of $\mathcal{G}$.

3.3 Data analysis

During steady state crack propagation, one expects the energy release rate to be uniquely related to the crack velocity by the classical empirical equation first established by Maugis and Barquins[37] and inspired by early studies of Gent[16] and Kinloch:[38,39]

$$\mathcal{G} = \mathcal{G}_0\left[1 + \left(\frac{v}{v^*}\right)^n\right] \quad (2)$$

where $\mathcal{G}_o$ is the threshold or thermodynamic work of adhesion, v is the crack velocity at the interface, v^* is the critical velocity giving rise to viscoelastic energy dissipation and n is the adhesion exponent. We remark that $\mathcal{G} \approx \mathcal{G}_0$ for $v \ll v^*$.

Eqn (2) was established to describe adhesion of elastic rubbers to solid surfaces.[40] It assumes that the energy required to propagate a crack is given by the sum of the thermodynamic work of adhesion $\mathcal{G}_0$ and the energy dissipated due to viscoelasticity. It has been shown empirically that the dissipated energy is a power law over a wide range of crack propagation velocities. According to this classical interpretation, the contributions of the interfacial interactions and of the material rheology are substantially decoupled: $\mathcal{G}_0$ should only depend on the nature of the interface, while n and v^* should only depend on the viscoelastic rheological properties of the adhesive. However, a quantitative link between n, v^* and the rheological properties has not been established so far. From the experimental data of $\mathcal{G}$ *vs.* v, it is in principle possible to estimate the three fitting parameters in eqn (2) – $\mathcal{G}_0$, v^* and n. However, in most practical conditions values of v^* and $\mathcal{G}_0$ cannot be accurately estimated independently because the crossover region where $\mathcal{G} \approx \mathcal{G}_0$ for $v \ll v^*$ is rarely observed. In fact, small propagation velocities are difficult to be reliably measured for low values of the applied $\mathcal{G}$ as steady state propagation cannot be observed over long times in the presence of viscoelastic relaxation. The most reasonable fit to the available data in Fig. 7 and 8 is a single power law for each data series. This physically means that the value of $\mathcal{G}$ for all data points is comfortably larger than $\mathcal{G}_0$, thus implying that the crack velocity is always larger than the critical velocity v^*. Eqn (2) is thus reduced to a two parameter approximated equation as follows:

$$\left(\frac{v}{v^*}\right)^n \gg 1 \quad \mathcal{G} = \mathcal{G}_0\left(\frac{v}{v^*}\right)^n = Av^n \quad (3)$$

Thus, the two empirical parameters used in this study are the adhesion exponent n and the prefactor $A = \frac{\mathcal{G}_0}{(v^*)^n}$. Since the dimensional unit of A depends on the value of the exponent n, the prefactor A cannot be used to directly compare the interfacial energy $\mathcal{G}_0$ between different samples unless the exponent n is identical. A global comparison of the $\mathcal{G}(v)$ curves in the available velocity range is thus the best option.

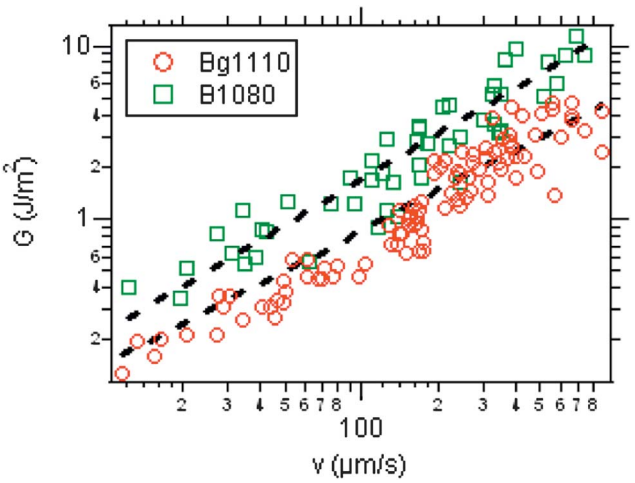

Fig. 7 Representative scatter plots of the energy release rate $\mathcal{G}$ calculated from eqn (1) and the crack-tip velocity v measured from the videos. Data shown here are for the adhesives Bg1110 (○) and B1080 (□) against COC. The small amount of scatter indicates a good reproducibility of the experiments. The fitted curves indicate a power law relationship between the two physical quantities $\mathcal{G}$ and v.

4 Results and discussions

4.1 Crack velocity v as a function of applied energy release rate $\mathcal{G}$

Using eqn (1) to obtain the energy release rate $\mathcal{G}$ and the estimate of the average propagation velocity v of the crack-tip

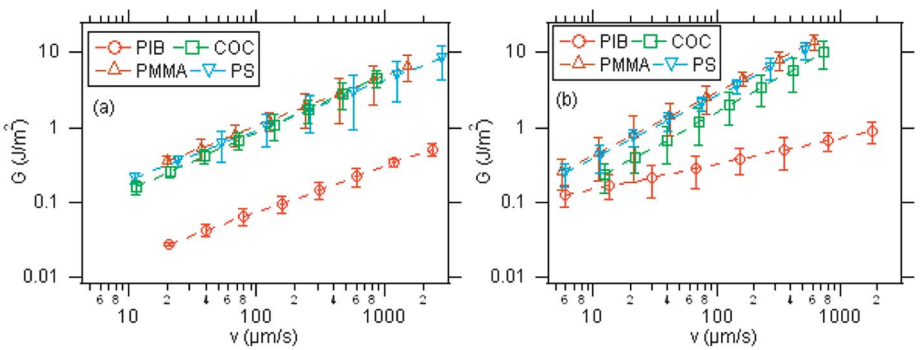

Fig. 8 Power law curves showing the energy release rate $\mathcal{G}$ against the crack-tip velocity v for the adhesives (a) Bg1110 and (b) B1080 against all tested surfaces.

discussed in Section 3.1, scatter plots of $\mathcal{G}$ *vs.* v for all sample/substrate combinations have been constructed. For the sake of simplicity, two representative plots consisting of data obtained from tests on the two model adhesives against COC are shown in Fig. 7. Their respective fits using the approximation given by eqn (3) are included as well. The data presented here are the outcome of 12 separate tests for Bg1110 and 6 tests for B1080. There are two important conclusions that can be drawn from these plots. First, the scatter in the $\mathcal{G}$ *vs.* v data points is quite small relative to the large variation of these variables which makes the approximations reasonable. Second, the data are consistent with a power law relationship, as shown by the fits, between the two physical quantities $\mathcal{G}$ and v without any levelling off in the lower $\mathcal{G}$ regime. Hence, the use of two parameters in eqn (3) to fit the data is justified. It should be noted that for the tests that were carried out at the lowest values of applied $\mathcal{G}$, the crack nucleated but only propagated over a certain small distance and then apparently stopped (within the resolution of the optical observation). This threshold behaviour is probably related to local stress relaxation and needs to be investigated further. These experiments are not included in the results of the following figures.

The power law fits for all sample/substrate combinations are shown in Fig. 8(a) and (b) for Bg1110 and B1080 respectively. The error bars on $\mathcal{G}$ shown here are the residuals obtained from the scatter plots such as the one in Fig. 7. By looking at Fig. 8(a) one can clearly see two families of curves. The first type of curve showing lower values of the energy release rate $\mathcal{G}$ corresponds to the rubbery substrate material PIB and indicates poor adhesion. On the other hand, the glassy polymers PS, PMMA and COC show a much slower crack propagation velocity for a given $\mathcal{G}$, indicating better adhesion between the adhesives and the substrates.

In Fig. 8(b), the adhesive B1080 also shows a lower adhesion on the rubbery PIB but the $\mathcal{G}$ *vs.* v curve has in addition a different slope compared to the same adhesive debonded from the other substrates. Adhesion of B1080 on the non-polar substrate COC is intermediate between the polar substrates PS and PMMA and the PIB substrate. The values of the power exponent n have been evaluated from the plots in Fig. 8 and are shown as bar charts in Fig. 9. The uncertainty on n has been estimated to be within 20%. Typically, for elastomers, values of $n \sim 0.5$–0.6 have been found,[37,40] so values around 0.8 are not surprising for these highly viscoelastic materials. The interpretation of the value of the other fit parameter $A = \mathcal{G}_0/(v^*)^n$ (*cf.* Eqn (3)) is complicated if n is not constant and cannot be seen as purely related to interfacial interactions. For example, in the case of Bg1110 where n values are similar thereby producing parallel slopes in Fig. 8(a), one can compare the values of A to estimate the ratio between the interfacial adhesion energies $\mathcal{G}_0$ against different surfaces. But, for B1080 where dissimilar values of n are observed in Fig. 8(b), A cannot represent an interfacial energy term since the two fitted parameters are coupled as discussed in Section 3.3, and both n and v^* should carry information from the rheology of the adhesive.

Regardless of the model used, the $\mathcal{G}(v)$ curves in Fig. 8 are direct measurements of the adhesion of the two model adhesives on the different surfaces. The different values of $\mathcal{G}$ for a given crack velocity on different substrates indicate very different levels of dissipated energy for the same average strain rate applied near the crack tip. This is a surprising result as the differences in the values of $\mathcal{G}_0$ are expected to be small between the tested surfaces. These different values can also not be attributed to the adhesive material properties as strong differences are observed for a given material on different substrates. They have thus to be related either to differences in the geometry of the crack or to differences in the size of the dissipative volume. The same holds for the equally surprising observation of different exponents n found for the B1080.

The behaviour of Bg1110 is very similar to the expected behaviour of a weakly crosslinked elastomer. The same qualitative behaviour is observed for the B1080 with the exception of the difference in n between adhesion on rubbery and glassy substrates. Comparing the values of $\mathcal{G}$ in Fig. 8 for the two adhesives on the same substrate shows a tendency for the B1080 to have a higher value of measured $\mathcal{G}$ for the same crack velocity reflecting the difference in polymer architecture and the rheological properties leading to a higher level of energy dissipation. This result is qualitatively consistent with the results found in probe tack tests.[10]

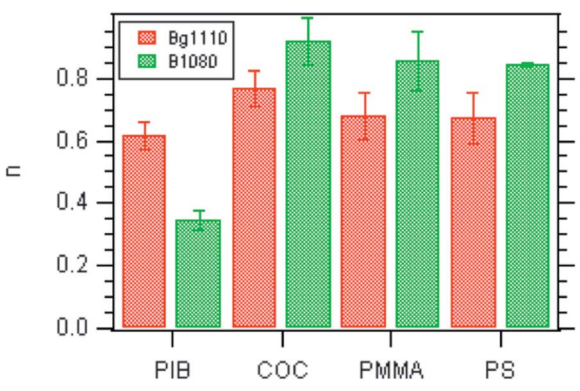

Fig. 9 Bar charts representing the values of the power coefficient n of the adhesives Bg1110 and B1080 against all the tested substrates. Values of n greater than 0.6 indicate viscoelastic energy dissipation. The values of n for B1080 against the rubbery substrate PIB is different from other substrates. This could indicate a different dissipative mechanism possibly due to a change in boundary conditions.

4.2 Debonding contact angle measurement

Previous peel measurements speculated that the reason for large differences in adhesion energy could be due to differences in the steady-state contact angle between the adhesive and the substrate.[6] However direct measurements of the contact angle have been elusive and only a few studies have been able to give an estimate. Previous studies on PDMS model adhesives have shown that the contact angle during debonding strongly depends on the properties of the viscoelastic material and become markedly different from 90° for very soft adhesive materials which are able to flow and cannot store much elastic energy.[10] On the other hand, for well crosslinked elastic materials, a pure interfacial debonding results in a contact angle close to 90°.

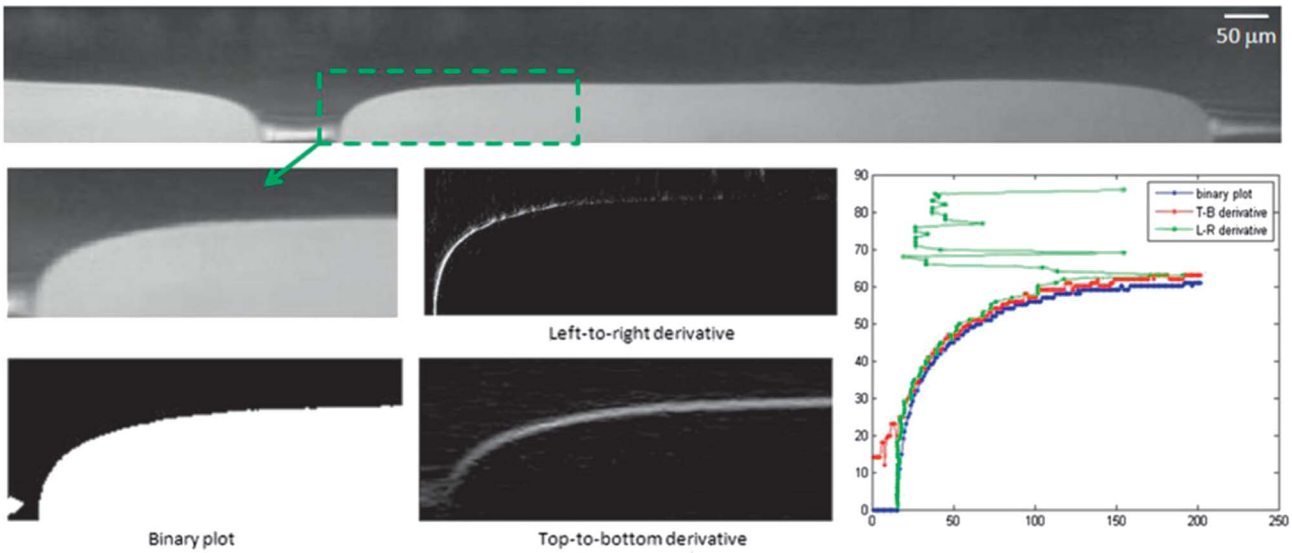

Fig. 10 Representative images showing the boundary of the crack front obtained from the debonding of Bg1110 against COC. Image analyses using MATLAB indicate a contact angle close to 90° which was true for all sample/substrate combinations used in this study.

In order to measure the contact angle, we have extracted the crack opening profile using MATLAB. Fig. 10 shows a representative crack propagation of Bg1110 against COC corresponding to an applied displacement $\delta = 40$ μm along with the extracted crack geometry. Routine MATLAB codes have been used to analyze the image. The contact angle has been measured by drawing a tangent at the triple point, *i.e.* at the interface of the adhesive, air and the substrate. The analysis of the crack opening profile estimates the contact angle to be $90 \pm 3°$ for both the adhesives against COC, PMMA and PS. For the PIB substrate, the propagation occurs at very small values of δ (<20 μm) and it was not possible to accurately extract the contact angle within the resolution of our camera. For our relative elastic materials we thus observe no deviation of the contact angle from 90° and differences in the contact angle are thus not at the origin of the observed differences in the energy release rate.

5 General discussion

The results presented above, obtained with the new sticky wedge device, provide new insights into the debonding mechanism of soft and highly viscoelastic materials and several points are worthy of a specific discussion. The striking difference between the adhesion on PIB and on the glassy polymers is in qualitative agreement with an earlier experimental report showing the effect of a change in substrate on adhesion of well crosslinked PnBA elastomers.[40,41] Ahn and Shull showed that the difference between debonding energy from a rubbery and a glassy substrate was primarily related to a change in v^* rather than $\mathcal{G}_0$. Other studies have shown that a polymer layer with a high surface mobility combined with low miscibility between the adhesive and the substrate gives rise to interfacial slippage and hence to a high crack-tip velocity at a given applied $\mathcal{G}$.[6,42–45] In our system $\mathcal{G}_0$ and v^* cannot always be separated but the qualitative consistency between the results obtained with fully viscoelastic and realistic adhesives, and those of Ahn and Shull obtained with JKR test on elastomers made from the same monomer are obvious. It is interesting to remark that the large observed differences in the adhesion energy release rate for different combinations of the adhesives and the substrates cannot be attributed to differences in the interfacial free energy $\mathcal{G}_0$. Even if the direct determination of $\mathcal{G}_0$ was not possible in our tests due to the very slow relaxation of our adhesives,[46,47] the variations of interfacial free energy between polymers (with the exception of fluorinated polymers) are very weak. As a very rough comparison between our model adhesives and other well-known polymers, we verified that wetting contact angles of water drops are substantially close to 90° as on most polymers (*cf.* measurements in Table 1). The large differences observed in the adhesion energy release rate for different combinations of adhesives and substrates must then be attributed to variations of v^* and are thus associated with energy dissipation mechanisms, such as the effect of the different resistance to interfacial slippage or to changes in the volume of the viscoelastic dissipation region.[6,42,43]

Another interesting result concerns the value of the adhesion exponent n. Previous studies on adhesion of elastomers on solid surfaces have always reported values of n controlled by the rheological properties of the adhesive only.[16,38,40] What is new and surprising in this study is the low value of n for B1080 against PIB. *As a consequence, there could thus be an unexpected dependence of n on an interfacial property.* The variation of n for the same adhesive on different substrates remains a very interesting and unexplained phenomenon, which would require further investigation on smaller scales in order to understand the changes in the mechanisms of energy dissipation.

Another hypothesis to explain the differences in adhesion energy is that although the measurements of the contact angle during debonding of the adhesives did not show large

variations from 90°, it is possible that a relevant change of the contact angle might have occurred at a much smaller scale which is out of reach of the present visualization equipment.

6 Conclusions

This study presents a new technique based on a wedge geometry to estimate the energy dissipated by a crack propagating at the interface between two model soft *highly viscoelastic* polymers and several different rigid surfaces. The local loading condition is analogous to a pure shear geometry and thus allows the measurement of the propagation velocity of a well defined crack front over significant distances at a nearly constant value of the applied energy release rate.

While the 2D geometry used in this study for the estimate of $\mathcal{G}$ is clearly an approximation, it has the advantage of fixing the debonding geometry better than the peel test and compels a directional propagation better than the axisymmetric probe test. With a possibility to improve the approximations for estimating the applied $\mathcal{G}$,[48–50] it is a promising method to investigate more quantitatively dissipative processes at or near interfaces for soft viscoelastic materials.

Two model pressure sensitive adhesives (PSA) consisting of random copolymers of poly(*n*-butyl acrylate-*co*-acrylic acid) with different molecular weights and branching levels have been used. The debonding experiment performed was a measurement of the interfacial crack-tip velocity under different conditions of the applied energy release rate on different model substrates. The applied energy release rate $\mathcal{G}$ (estimated with a pure shear approximation) was related to the crack-tip velocity v as follows:

$$\mathcal{G} = Av^n$$

The values of A and n have been calculated using curve fitting. Adhesion of both adhesives on the rubbery polyisobutylene (PIB) is significantly lower than on glassy materials despite very similar surface energies. Amongst the glassy materials, more polar substrates display higher adhesion energies against the two model adhesives.

The measured energy release rates for these viscoelastic materials could clearly discriminate between the two adhesives on the same surfaces and showed the importance of viscoelastic dissipation for the measured adhesive energy. Interestingly, the adhesive B1080 which is more viscoelastic appears to have two distinct values of the exponent n depending on whether the adhesion is weak or strong. This hints at a change in the boundary condition when going from strong to weak adhesion. However, within the experimental resolution, it was not possible to accurately determine the contact angle for lower adhesion.

Acknowledgements

The authors would like to acknowledge the European Union for funding through the MODIFY project (NMP grant agreement no. 228320). Additional financial support has been provided by The Dow Chemical Company. CC is grateful to Thomas Schweizer, ETH Zurich for providing the TOPAS® COC. Rheology experiments were performed at Université Catholique de Louvain, Belgium and the contributions of Christian Bailly, Dietmar Auhl and Lalaso Mohite were of immense help.

References

1 C. Creton and E. Papon, *MRS Bull.*, 2003, **28**, 419–421.
2 C. Creton, *MRS Bull.*, 2003, **28**, 434–439.
3 L. Léger and C. Creton, *Philos. Trans. R. Soc., A*, 2008, **366**, 1425–1442.
4 T. Tang, A. Jagota, M. K. Chaudhury and C.-Y. Hui, *J. Adhes.*, 2006, **82**, 671–696.
5 J. Nase, A. Lindner and C. Creton, *Phys. Rev. Lett.*, 2008, **101**, 4.
6 B. Z. Newby, M. K. Chaudhury and H. R. Brown, *Science*, 1995, **269**, 1407–1409.
7 D. Ahn and K. R. Shull, *Langmuir*, 1998, **14**, 3637–3645.
8 K. R. Shull, *J. Polym. Sci., Part B: Polym. Phys.*, 2006, **44**, 3436–3439.
9 A. N. Gent, *Langmuir*, 1996, **12**, 4492–4496.
10 J. Nase, C. Creton, O. Ramos, L. Sonnenberg, T. Yamaguchi and A. Lindner, *Soft Matter*, 2010, **6**, 2685–2691.
11 T. Yamaguchi, K. Koike and M. Doi, *Europhys. Lett.*, 2007, **77**, article 64002.
12 C. Derail, A. Allal, G. Marin and P. Tordjeman, *J. Adhes.*, 1997, **61**, 123–157.
13 A. Ghatak, L. Mahadevan and M. K. Chaudhury, *Langmuir*, 2005, **21**, 1277–1281.
14 A. Ahagon and A. N. Gent, *J. Polym. Sci., Part B: Polym. Phys.*, 1975, **13**, 1903–1911.
15 A. Ahagon and A. N. Gent, *J. Polym. Sci., Part B: Polym. Phys.*, 1975, **13**, 1285–1300.
16 A. N. Gent and J. Schultz, *J. Adhes.*, 1972, **3**, 281–294.
17 A. J. Crosby, K. R. Shull, H. Lakrout and C. Creton, *J. Appl. Phys.*, 2000, **88**, 2956–2966.
18 C. Creton, J. Hooker and K. R. Shull, *Langmuir*, 2001, **17**, 4948–4954.
19 A. Lindner, T. Maevis, R. Brummer, B. Luhmann and C. Creton, *Langmuir*, 2004, **20**, 9156–9169.
20 F. Deplace, C. Carelli, S. Mariot, H. Retsos, A. Chateauminois, K. Ouzineb and C. Creton, *J. Adhes.*, 2009, **85**, 18–54.
21 P. L. Drzal and K. R. Shull, *J. Adhes.*, 2005, **81**, 397–415.
22 K. R. Shull and C. Creton, *J. Polym. Sci., Part B: Polym. Phys.*, 2004, **42**, 4023–4043.
23 Y. Urahama, *J. Adhes.*, 1989, **31**, 47–58.
24 A. Lindner, B. Lestriez, S. Mariot, C. Creton, T. Maevis, B. Luhmann and R. Brummer, *J. Adhes.*, 2006, **82**, 267–310.
25 A. Zosel, *J. Adhes.*, 1989, **30**, 135–149.
26 C. Verdier, J. M. Piau and L. Benyahia, *J. Adhes.*, 1998, **68**, 93–116.
27 J. Teisseire, F. Nallet, P. Fabre and C. Gay, *J. Adhes.*, 2007, **83**, 613–677.
28 G. Haiat, M. C. Phan Huy and E. Barthel, *J. Mech. Phys. Solids*, 2003, **51**, 69–99.
29 G. Josse, P. Sergot, C. Creton and M. Dorget, *J. Adhes.*, 2004, **80**, 87–118.
30 T. Ondarçuhu, *J. Phys.*, 1997, **7**, 1893–1916.

31 E. P. Chang, *J. Adhes.*, 1991, **34**, 189–200.
32 F. Saulnier, T. Ondarçuhu, A. Aradian and E. Raphael, *Macromolecules*, 2004, **37**, 1067–1075.
33 L. V. Mohite, D. Auhl, M. Ahmadi, J. T. Padding, C. Bailly, F. Tanguy and C. Creton, *submitted to J. Rheol.*, 2013.
34 J. T. Padding, L. V. Mohite, D. Auhl, T. Schweizer, W. J. Briels and C. Bailly, *Soft Matter*, 2012, **8**, 7967–7981.
35 C. Creton and L. Leibler, *J. Polym. Sci., Part B: Polym. Phys.*, 1996, **34**, 545–554.
36 R. S. Rivlin and A. G. Thomas, *J. Polym. Sci.*, 1953, **10**, 291–318.
37 D. Maugis and M. Barquins, *J. Phys. D: Appl. Phys.*, 1978, **11**, 1989.
38 E. H. Andrews and A. J. Kinloch, *Proc. R. Soc. London, Ser. A*, 1973, **332**, 401–414.
39 E. H. Andrews and A. J. Kinloch, *J. Polym. Sci., Polym. Symp.*, 1974, **46**, 1–14.
40 D. Ahn and K. R. Shull, *Langmuir*, 1998, **14**, 3646–3654.
41 D. Ahn and K. R. Shull, *Macromolecules*, 1996, **29**, 4381–4390.
42 B. Z. Newby and M. K. Chaudhury, *Langmuir*, 1997, **13**, 1805–1809.
43 B. Z. Newby and M. K. Chaudhury, *Langmuir*, 1998, **14**, 4865–4872.
44 N. Amouroux, J. Petit and L. Léger, *Langmuir*, 2001, **17**, 6510–6517.
45 R. Schach, Y. Tran, A. Menelle and C. Creton, *Macromolecules*, 2007, **40**, 6325–6332.
46 *Physical Properties of Polymers*, ed., J. E. Mark, American Institute of Physics, Woodbury, New York, 1996.
47 K. L. Johnson, K. Kendall and A. D. Roberts, *Proc. R. Soc. London, Ser. A*, 1971, **324**, 301–313.
48 M. Barquins, *J. Adhes.*, 1988, **26**, 1–12.
49 M. K. Chaudhury, T. Weaver, C. Y. Hui and E. J. Kramer, *J. Appl. Phys.*, 1996, **80**, 30–37.
50 F. Robbe-Valloire and M. Barquins, *Int. J. Adhes. Adhes.*, 1998, **18**, 29–34.